NASA/TM—1999-209079

# Development of Refractory Silicate-YSZ Dual Layer TBCs

Yirong He, Kang N. Lee, and Surendra Tewari
Cleveland State University, Cleveland, Ohio

Robert A. Miller
Glenn Research Center, Cleveland, Ohio

National Aeronautics and
Space Administration

Glenn Research Center

July 1999

## Acknowledgments

We are grateful to George Leissler and Gary Kostyak of Dynacs, NASA Glenn group, for processing sprayed and sputtered coatings, respectively. We are also thankful to Northwestern University for the supply of SPPS coatings. This work was supported by DOE AGTSR program under the contract number 96-01-SR042.

Available from

NASA Center for Aerospace Information
7121 Standard Drive
Hanover, MD 21076
Price Code: A03

National Technical Information Service
5285 Port Royal Road
Springfield, VA 22100
Price Code: A03

# DEVELOPMENT OF REFRACTORY SILICATE-YSZ DUAL LAYER TBCs

Yirong He, Kang N. Lee, and Surendra Tewari
Cleveland State University
Cleveland, OH 44115

Robert A. Miller
NASA Glenn Research Center
21000 Brookpark Road
Cleveland, OH 44135

**Abstract**

Development of advanced thermal barrier coatings (TBCs) is the most promising approach for increasing the efficiency and performance of gas turbine engines by enhancing the temperature capability of hot section metallic components. Spallation of the yttria-stabilized zirconia (YSZ) top coat, induced by the oxidation of the bond coat coupled with the thermal expansion mismatch strain, is considered to be the ultimate failure mode for current state-of-the-art TBCs. Enhanced oxidation resistance of TBCs can be achieved by reducing the oxygen conductance of TBCs below that of thermally grown oxide (TGO) alumina scale. One approach is incorporating an oxygen barrier having an oxygen conductance lower than that of alumina scale. Mullite, rare earth silicates and glass ceramics have been selected as potential candidates for the oxygen barrier. This paper presents the results of cyclic oxidation studies of oxygen barrier/YSZ dual layer TBCs.

## 1. Introduction

Thermal barrier coatings (TBCs) will play an essential role in the development of a new generation of land-based gas turbine systems with higher efficiency, longer lifetime, and lower cost (Ref 1). Current state-of-the-art TBCs typically consist of a metallic bond coat and an yttria-stabilized zirconia (YSZ) top coat. Studies have shown that oxidation of the bond coat is primarily responsible for the failure of the current state-of-the-art TBCs (Ref 2 and 3). This implies that the performance of TBCs can be improved by reducing the oxidation rate of the bond coat and/or by enhancing the adhesion of the thermally grown oxide (TGO). Based on this idea, much research has been carried out to understand the factors that affect the oxidation kinetics and alumina scale adhesion (Ref 4-6). Pint, et. al. investigated the important factors for achieving an adherent $Al_2O_3$ scale in commercial TBC systems. An EB-PVD YSZ coating on a bulk β-NiAl+Zr alloy showed a lifetime increased by a factor of five compared to a standard Pt aluminide/EB-PVD YSZ on Rene N5 (Ref 6). The increased lifetime was attributed to improved scale adhesion. Sun, et al. (Ref 7) and Schmitt-Thomas, et al. (Ref 8) investigated a sealing concept by applying an intermediate $Al_2O_3$ diffusion barrier between the bond coat and the top YSZ coat. The thermal cyclic life at 1000°C with an $Al_2O_3$ intermediate layer was improved by a factor of two to four (Ref 7and 8).

Chang et al. (Ref 9) and Phucharoen (Ref 10) used a finite element model to quantify the nature of the stress build-ups in plasma-sprayed YSZ TBCs with an idealized sinusoidally rough interface between the ceramic and bond coat during a single cooling cycle. Thermal expansion mismatch generated tensile radial stresses in combination with compressive in-plane stresses in the YSZ near the tip of the peaks and compressive stresses in the valley region. In contrast, oxidation produced tensile stresses in the valleys and compressive stresses in the peak regions. Freborg et al. included bond coat and top coat creep and multiple thermal cycles in their finite element model to characterize the stresses in plasma-sprayed YSZ TBCs (Ref 11). Their results indicated that top coat and bond coat creep also contributed to the generation of tensile stresses at the bond coat peak and off-peak location and compressive stresses in the valley regions. Thus, the suggested evolution of residual stresses in plasma-sprayed TBCs is as follows: Early cracking at the bond coat peak is due to thermal expansion mismatch and creep, because thermal expansion mismatch and creep produce tension in the peak region and compression in the valley region. These cracks do not propagate due to the compressive stresses over the valley region. With increase in the number of cycles and TGO

thickness, stresses over the valley become increasingly tensile. When tensile stresses over the valley region are high enough to sustain the crack growth, cracks at the peak link together and delamination occurs. Thus the growth of TGO accelerates the TBC failure. Cheng and his colleagues (Ref 12) have used elastic-plastic finite element analysis to compute the thermal/residual stresses in a disk-shaped test specimen consisting of an electron beam physical vapor deposited YSZ TBC on a Pt-Al bond coat and Ni-based superalloy substrate. Actual interface geometry was used to generate finite element models. It was found that the largest stress occurred in the TGO layer. Irregular interfaces lead to large vertical tensile stresses in the TGO.

It is believed that improved oxidation resistance of TBCs can be achieved by incorporating an oxygen barrier having an oxygen conductance lower than that of TGO alumina between the top YSZ coat and the bond coat. Rare-earth silicates, such as $La_2SiO_5$, $Sm_2SiO_5$, $Y_2SiO_5$, glass ceramics, such as CAS (Calcia-Alumina-Silicate), BAS (Baria-Alumina-Silicate) and mullite are promising as an oxygen barrier because of their low oxygen conductivity.

High velocity oxygen fuel (HVOF) thermal spraying, a new variant in thermal spray technology, exhibits the following advantages: 1) the high particle velocity renders a dense coating with higher adhesive and cohesive strength than its plasma sprayed counterpart; 2) HVOF sprayed coatings have low surface roughness; and 3) less thermally induced changes are generated in the coating material compared to plasma sprayed coating (Ref 13 and 14). This technology has been used in spraying MCrAlY coating (Ref 15), carbide coating (Ref 14) and YSZ coating (Ref 16). In this study, HVOF, air plasma spray (APS), sputtering and small particle plasma spray (SPPS, Northwestern University) were used to apply the oxygen barrier coatings. This paper summarizes the preliminary results of the development of oxygen barrier coatings.

## 2. Experimental Procedure

Plasma spray grade powders of BAS, CAS, $Y_2SiO_5$, $La_2SiO_5$, and $Sm_2SiO_5$ were processed by commercial vendors (Zirtech, Niagara Fall, NY and MO-SCI Corporation, Rolla, MO). Plasma spray grade mullite powder (50~100 micron particle size) was purchased from Cerac (Milwaukee, WI). Sub-micron mullite powders for SPPS were purchased from Baikowski International (Charlotte, NC). A mullite target for sputtering was fabricated at Target Materials Inc. (Columbus, OH).

The standard TBCs in this study consisted of a 0.25mm thick $ZrO_2$-8 wt%$Y_2O_3$ (YSZ) top coat and 0.15mm thick Ni-36Cr-6Al-0.5Y bond coat on grit blasted CMSX4+Y substrate (25mm in diameter and 3mm in thickness). The YSZ top coat was deposited using APS. Low pressure plasma spray (LPPS) was used to apply the bond coat. All coatings were sprayed on one face of the substrates.

HVOF and APS were used to apply thick (50~75 μm) oxygen barrier coatings. Table 1 lists the HVOF and APS spray parameters for oxygen barrier coatings. Thin (1~10μm) oxygen barrier coatings were deposited by sputtering and SPPS.

As-sprayed coupons were annealed at 1100°C-1150°C in Ar-5% $H_2$ for 4 hours. Thermal cyclic testing was performed at 1100°C-1150°C using box furnaces or automated cyclic furnaces. Three cycling conditions were selected for the oxidation test: 1h cycle (1h high temperature-15 min room temperature), 20h cycle (20h high temperature-20 min room temperature) and 100h cycle (100h high temperature-20 min room temperature). Typically, samples reached the high temperature within 2 min and the low temperature within 5 min in each cycle.

X-ray diffractometry (XRD) was used to identify the phases present in the coating. Surface morphology and cross-sections of the coating were examined using scanning electron microscopy (SEM) equipped with energy dispersive spectrometry (EDS) attachment.

## 3. Results and Discussion

### 3.1. Selection of Oxygen Barrier

Low oxygen conductivity, chemical compatibility, and high coefficient of thermal expansion (CTE) were the three key factors in determining the selection of new ceramic materials. Since few ceramics meet all three requirements, some low CTE ceramics were selected as long as they met the other two criteria. The CTEs of the substrate, bond coat, $Al_2O_3$ and the selected materials are listed in Table 2. X-ray diffraction was used to identify the phases in as-received powders, and the results are listed in Table 3.

### 3.2. Development of Coating Application Technology

A previous study (Ref 17) indicated that refractory silicates and glass ceramics have the tendency to form amorphous or metastable phases, which are unstable at high temperatures, and phase transformations to stable phases take place under thermal exposure. In many cases, these phase transformations are detrimental to the integrity of the coating due to the large volume changes accompanying the transformations (Ref 17 and 18). Heating the substrate above the phase transformation temperature suppressed the precipitation of amorphous or metastable phases and substantially enhanced the durability of silicate coatings (Ref 17). Thus, the selected coatings were applied onto heated (1100°C) substrates to investigate the effect of substrate temperature on the phase stability and the durability of TBCs.

Due to the relatively high surface roughness of conventional APS and HVOF coatings, it was not possible to deposit a thin oxygen barrier (<25 μm) with a complete coverage. Therefore, sputtering and SPPS were used to apply thin oxygen barrier coatings (1~10 μm).

### 3.3. Testing and Data Analysis

**Standard YSZ coating**

Figure 1a shows the cross-section of as-sprayed standard YSZ. This coating failed after 9 cycles of 100h cycle test at 1100°C and 11 and 17 cycles of 20h cycle test at 1100°C. At 1150°C, the coating failed after 10~18 cycles of 20h cycle test and 130 cycles of 1h cycle test. Figure 1b represents a typical cross-section of a standard YSZ coating after failure. Delamination was observed mainly within the YSZ top coat near the YSZ/TGO interface, while some occurred along the TGO/bond coat interface.

**Thick oxygen barrier coating (50~75μm)**

*BAS Coating*: HVOF-sprayed BAS/YSZ coatings debonded after annealing. The debonded interface was powdery. Cross-sectional examination (Fig. 2) revealed that the BAS coating was porous and incompletely melted. Figure 3a shows the cross-section of as-sprayed APS BAS/YSZ coating. It has a layered structure, especially towards the BAS/bond coat interface. The APS BAS/YSZ coating survived the annealing, but failed after 2 cycles of 20h cycle test at 1150°C. The failure occurred mainly along the BAS/YSZ interface as shown in Fig. 3b.

*Mullite Coating*: As-sprayed HVOF mullite/YSZ coating showed a partial delamination at the mullite/bond coat interface, and completely failed after a 1150°C/4 h anneal.

APS mullite coatings were applied on both heated (1100°C) and unheated substrates to investigate the effect of substrate temperature on the phase stability and the coating performance. Mullite was the only phase detected on as-sprayed coupons (heated and unheated). APS mullite coatings were dense with or without the substrate heating. Figure 4a shows an as-sprayed APS mullite/YSZ without substrate heating. This coating failed after 1 cycle of 20h cycle test at 1150°C. Branching cracks formed and propagated in the mullite coating as shown in Fig. 4b. It is believed that the amorphous mullite and the metastable alumina formed during the spraying and subsequently transformed to stable phases during the thermal cycling, causing the cracking. Trace amounts of $SiO_2$ and $Al_2O_3$ were detected by XRD in the mullite coating after 1 cycle of 20h cycle test at 1150°C. Mullite/YSZ coating applied on a heated substrate failed along the YSZ/mullite interface after annealing, indicating that the substrate heating did not lead to improved adhesion.

The premature failure of low CTE oxygen barrier coatings (BAS and mullite) is presumably due to stresses caused by their large CTE mismatch with the YSZ. Phase instability and the high Young's modulus of these coatings due to their high density are the other contributing factors to the stress. Applying a thin, low CTE coating may alleviate this problem because thinner coatings are more compliant.

*Rare Earth Silicate Coatings ($Y_2SiO_5$, $La_2SiO_5$, $Sm_2SiO_5$)*: HVOF-sprayed rare earth silicate coatings were porous and incompletely melted as shown in Fig. 5a. This resulted in the failure of the coatings after annealing or 1cycle of 20h cycle test at 1150°C. APS coatings were denser, but cracks were observed in the as-sprayed coating as shown in Fig. 5b. The APS $La_2SiO_5$/YSZ coatings failed after 2 cycles of 20h cycle test at 1150°C.

Figure 6a shows a cross section of as-sprayed APS $Sm_2SiO_5$ coating on heated substrate (1100°C). These coatings tended to develop large cracks parallel to the YSZ/$Sm_2SiO_5$ coating interface, and failed along the crack after annealing. Fig. 6b is a cross section of as-sprayed APS $Sm_2SiO_5$ coating on unheated substrate. Branching cracks formed in the coating. This coating failed within the $Sm_2SiO_5$ coating after 3 cycles of 20h cycle test at 1150°C. Figures 6c and 6d show the cross-sections of APS $Sm_2SiO_5$ coating on unheated substrate after the failure.

One key observation with these rare earth silicate coatings is that they cracked and failed prematurely despite the better CTE match. Also, substrate heating did not provide any improvement. The low thermal cycling resistance of rare earth silicate coatings may be due to their phase instability. XRD analysis was performed on $Y_2SiO_5$, $La_2SiO_5$, and $Sm_2SiO_5$ coatings to study the phase stability of these coatings. The results for $La_2SiO_5$ are listed in Table 4. $Y_2SiO_5$ and $Sm_2SiO_5$ showed a similar behavior. The as-sprayed $La_2SiO_5$ coating deposited on an unheated substrate was amorphous, whereas the single phase $La_2O_3$ was deposited when sprayed on a heated substrate. Both as-sprayed coatings transformed to $La_2SiO_5$ + $La_2O_3$ after annealing. After 5 cycles, $LaAlO_3$ phase appeared, presumably formed by the reaction between $La_2O_3$ and $Al_2O_3$. The low thermal shock resistance of the $La_2SiO_5$ coating was presumably due to stresses generated by the phase transformations and the CTE mismatch between the $La_2SiO_5$ and $La_2O_3$ that coexisted in the coating.

Heat treatments were performed on $La_2SiO_5$ powder to further investigate the phase stability. Powder was processed by fusion and grinding. Both as-solidified and ground $La_2SiO_5$ contained significant amount of $La_2O_3$, indicating some $La_2SiO_5$ decomposed to $La_2O_3$ + $SiO_2$ (amorphous) during the solidification. On heating, most of the $La_2O_3$ and $SiO_2$ readily reassociated to $La_2SiO_5$. A similar phenomenon was reported for $ZrSiO_4$ (Ref 19). Cooling rate (furnace cooling vs. air cooling) did not affect the phase transformation behavior of $La_2SiO_5$. A 1mm thick APS $La_2SiO_5$ stand-alone sample was obtained by spraying $La_2SiO_5$ onto graphite plate and subsequently burning off the graphite at 660°C in air. The coupon was annealed in Ar-5%$H_2$ for 4 hours at 1100°C before undergoing the 3 cycles of 20h cycle test at 1150°C. The results of XRD are shown in Table 4. $La_2SiO_5$ and $La_2O_3$ were the major phases after the graphite burn-off and annealing. After 3 cycles of 20h cycle test at 1150°C, most $La_2O_3$ reassociated to $La_2SiO_5$, similar to the behavior of $La_2SiO_5$ powder. The difference between the $La_2SiO_5$ coating and the bulk $La_2SiO_5$ was that the $La_2SiO_5$ coating retained a substantial amount of $La_2O_3$ after thermal exposure.

Figure 7 summarizes the cyclic oxidation durability of APS thick oxygen barrier/YSZ TBCs. All TBCs with thick oxygen barrier were inferior to the standard YSZ. The three bars for standard YSZ in Fig.7 represent the data for three coupons from three different batches.

**Thin oxygen barrier coating (1~10μm)**

Figure 8 is a cross-section of sputtered 3μm mullite/YSZ TBC after 8 cycles of 20h cycle test at 1100°C. A dense layer of TGO $Al_2O_3$ formed underneath the continuous mullite layer. Cracks formed in the YSZ near the mullite/YSZ interface and debonding was observed at the valley of mullite/YSZ interface. Failure occurred mostly in the YSZ near the YSZ/mullite interface (Fig. 8b), similar to the failure mode of standard TBCs. Sputtered 6 μm mullite/YSZ showed a similar behavior to the 3 μm mullite/YSZ. Figure 9 shows the X-ray map for Al, Si and O for the cross-section of sputtered 6 μm mullite/YSZ after failure (13 cycles of 20h cycle test at 1100°C), showing the TGO $Al_2O_3$ underneath the mullite. The thickness of TGO alumina was reduced by a factor of two in the presence of thin mullite oxygen barrier (Fig. 10).

Figure 11 shows the cross section of as-sprayed SPPS mullite coating. The bond coat was completely covered by the mullite coating, however, the coating thickness was not uniform. Further optimization is necessary to produce a uniform coating. The SPPS mullite/YSZ failed after 8 cycles of 20 h cycle test and 5 cycles of 100h cycle test at 1100°C.

Figures 12 and 13 show the lifetime of TBCs with thin oxygen barrier in 20h and 100h cycle test, respectively, at 1100°C. Thin mullite/YSZ TBCs showed durability comparable to that of standard TBC, demonstrating the potential of thin oxygen barrier coatings.

Even though the sputtered and SPPS thin mullite coatings performed far better than the thick APS mullite coatings with significantly reduced bond coat oxidation rates, there was no improvement in the coating life compared to standard YSZ TBCs. It is interesting to note that at the time of failure, the combined thickness of mullite and TGO in the thin mullite/YSZ TBC (Fig. 10b) was about same as the thickness of TGO in the standard TBC (Fig. 10a). It appears that the mullite coating, due to its low CTE and high Young's modulus, acted like TGO in generating tensile stresses. Thus, the mullite/YSZ TBC failed when the combined thickness of mullite + TGO

reached the thickness of TGO in standard TBC at the time of failure. This indicates that higher CTE and lower modulus are required for the oxygen barrier to minimize the stress generation by the oxygen barrier.

## 4. Summary and Conclusions

The HVOF-sprayed oxygen barrier coatings tended to be incompletely melted and powdery, while APS-sprayed oxygen coatings were denser. As a result, the HVOF coatings were in general inferior to APS coatings.

TBCs with a thick (50 ~ 75 μm), low CTE oxygen barrier coating (mullite, BAS,CAS) tended to delaminate within the oxygen barrier coating or at the YSZ/low CTE coating interface, presumably due to the CTE mismatch stress. This indicates the need for thin coatings to reduce the CTE mismatch stresses. Microcracks were observed in the APS-sprayed thick (50 ~ 75 μm) rare earth silicate coatings. On thermal cycling, the rare earth silicate coatings failed prematurely by developing more cracks. Phase instability appeared to be the major contributor to the lack of thermal shock resistance.

Thin mullite oxygen barrier coatings (1 ~ 10 μm) reduced the oxidation rate of bond coat by two folds. The durability of sputtered or SPPS thin mullite/YSZ TBCs was far better than that of thick APS mullite/YSZ TBCs. However, the life of the sputtered or SPPS mullite/YSZ TBCs was still similar to that of standard TBCs, suggesting that improved oxidation resistance alone was not sufficient for enhanced TBC durability. The low CTE and high elastic modulus of mullite appear to be responsible for the lack of lifetime improvement in thin mullite/YSZ TBCs. Future work will be focused on thin oxygen barrier with high CTE and low modulus.

## References


1. W. P. Parks, E. E. Hoffman, W. Y. Lee, and I. G. Wright, "Thermal Barrier Coatings Issues in Advanced Land-Based Gas Turbines", Proceedings of Thermal Barrier Coating Workshop, NASA Conference Publication 3312 (1995) 35-47.
2. R. A. Miller and C. E. Lowell, "Failure Mechanisms of Thermal Barrier Coatings Exposed to Elevated Temperatures", Thin Solid Films, 95 (1982) 265-273.
3. R. A. Miller, " Oxidation-Based Model for Thermal Barrier Coating Life", J. Am. Ceram. Soc., 67 (1984) 517-521.
4. R. A. Miller, " Thermal Barrier Coatings for Aircraft Engines-----History and directions", Proceedings of Thermal Barrier Coating Workshop, NASA Conference Publication 3312 (1995) 17-34.
5. J. Schaeffer, " The Effect of Alumina Phase Transformations on Thermal Barrier Coating Durability", Proceedings of TBC Interagency Coordination Committee, (1997) 99-108.
6. B. A. Pint, I. G. Wright, W. Y. Lee, Y. Zhang, K. Pruβner, K.B. Alexander, "Substrate and bond coat compositions: factors affecting alumina scale adhesion", Materials Science and Engineering, A245 (1998) 201-211.
7. J. Sun, E. Chang and B. Wu, " Performance of CVD $Al_2O_3$ Intermediate Layer between Zirconia Top Coat and NiCrAlY Bond Coat", Materials Transactions JIM, 34 No. 7 (1993) 614-631.
8. Kh. G. Schmitt-Thomas, U. Dietl and H. Haindl, " New Developments in Thermal Barrier Coatings (TBC) for gas Turbine Use", Industrial Ceramics, 16 No. 3 (1996) 195-198.
9. G. C. Chang, W. A. Phucharoen, R.A. Miller, "Behavior of Thermal Barrier Coatings for Advanced Gas Turbine Blades", Surface and Coating technology, 30 (1987) 13-28.
10. W. A. Phucharoen, Ph. D. Dissertation, Cleveland State University, Cleveland, OH 1990.
11. A. M. Freborg, B. L. Ferguson, W. J. Brindley, G. J. Petrus, " Modeling Oxidation induced stresses in Thermal Barrier Coatings", Materials Science and Engineering, A245 (1998) 182-190.
12. J. Cheng, E. H. Jordan, B. Barber and M. Gell, "Thermal/Residual Stress in an Electron beam Physical Vapor Deposited Thermal Barrier Coating System", Acta Mater. 46[16] (1998) 5839-5850.
13. O. C. Brandt, "Mechanical Properties of HVOF Coatings", J. Thermal Spraying Technology, 4[2] (1995) 147-152.
14. D. Lee, "Development of a Thick Wear-Resistant Jet Kote Coating Produced at High Deposition Rate: A Technical Note. J. Thermal Spray Technology, 4[3] (1995) 229-234.

15. H. van Esch and W. Greaves, "A Comparison of HVOF and LPPS Applied MCrAlY Coating", Proceedings of the International Gas Turbine and Aeroengine Congress and Exhibition, Birmingham, UK, June 10-13, (1996) 1-5.
16. Advanced Materials and Processes, "HVOF Spraying of Thermal Coatings", Metallurgia, 62[3] (1995) 136.
17. K. N. Lee, R. A. Miller and N. S. Jacobson, "New Generation of Plasma-Sprayed Mullite Coatings on Silicon Carbide", J. Am. Ceram. Soc., 78 [3] (1995) 705-710.
18. G. N. Heintz and U. Uematsu, "Preparation and Structures of Plasma-Sprayed $\gamma$ and $\alpha$-$Al_2O_3$ Coatings", Surface and coating Technology, 50 (1992) 213-222.
19. C. E. Curtis and H.G. Sowman, "Investigation of the Thermal Dissociation, Reassociation, and Synthesis of Zircon", J. Am. Ceram. Soc., 36 (1953) 190-198.

**Table 1 HVOF and APS Spraying Parameters for Oxygen Barrier Coatings**

| HVOF | | | | | | |
|---|---|---|---|---|---|---|
| Torch | Oxygen flow | Propylene flow | Air flow | Powder feed rate | Stand-off distance | Powder feed rate |
| Diamond Jet Hybrid | 606 SCFH# | 167 SCFH | 536 SCFH | 35 g/min | 25.4 cm | 50 cm/s |
| **APS** | | | | | | |
| Powder particle size | Gun power | Plasma gas flow | Carrier gas flow | Powder feed rate | Stand-off distance | Traverse speed |
| - 200 mesh | 45 kW | 14.4SLPM*Ar/9.6 SLPM He | 6 SLPM | 15 g/min | 15 cm | 30 cm/s |
| # Standard Cubic Foot Per Hour, * Standard Liter Per Minute | | | | | | |

**Table 2 CTEs of CMSX4+Y, NiCrAlY, $Al_2O_3$, Selected Ceramics and YSZ**

| Material | CMSX4+Y | NiCrAlY | $Al_2O_3$ | BAS, CAS, Mullite | $Y_2SiO_5$ | $La_2SiO_5$, $Sm_2SiO_5$ | YSZ |
|---|---|---|---|---|---|---|---|
| CTE ($10^{-6}$/°C) | 14-16 | 12-16 | 8-9 | 3-5 | 7-8 | 9-12 | 10 |

**Table 3 XRD Results of As-Received Powders**

| Powder | BAS | CAS | Mullite | $Y_2SiO_5$ | $La_2SiO_5$ | $Sm_2SiO_5$ |
|---|---|---|---|---|---|---|
| Phase | Celsian | Anorthite | Mullite | $Y_2SiO_5$ | $La_2SiO_5 + La_2O_3$ (minor) | $Sm_2SiO_5$ |

**Table 4 Summary of XRD Results of $La_2SiO_5$**

| Coupon | Heat treatment condition | XRD results |
|---|---|---|
| $La_2SiO_5$ heated | APS sprayed | $La_2O_3$ |
| | annealed* | $La_2SiO_5 + La_2O_3$ |
| | 1 cycle** | $La_2SiO_5 + La_2O_3$ |
| | 5 cycle | $LaAlO_3 + \alpha\text{-}Al_2O_3 + La_2SiO_5$ |
| | 10 cycle | $\alpha\text{-}Al_2O_3 + LaAlO_3 + NiAl_2O_4 + LaAlSi_2O_6$ |
| $La_2SiO_5$ unheated | APS sprayed | amorphous |
| | annealed | $La_2SiO_5 + La_2O_3$ |
| | 2 cycles | $La_2SiO_5 + La_2O_3$ |
| $La_2SiO_5$ powder | as received (-140/+200) | $La_2SiO_5$, $La_2O_3$ both major |
| | 1150°C/4 h | $La_2SiO_5 + La_2O_3$ (minor) |
| | 1150°C/20 h | $La_2SiO_5 + La_2O_3$ (minor) |
| | 1200°C/1 h | $La_2SiO_5 + La_2O_3$ (minor) |
| | 1200°C/24 h | $La_2SiO_5 + La_2O_3$ (minor) |
| | 1300°C/24 h in air | $La_2SiO_5$ |
| | 1400°C/24 h in air | $La_2SiO_5$ |
| | 1500°C/1 h | $La_2SiO_5 + La_2O_3$ (very minor) |
| | 1500°C/24 h | $La_2SiO_5$ |
| Powder after1300°C/24h in air | 1150°C/20 hr, air quench | $La_2SiO_5$ |
| | 1150°C/20 hr, furnace cooling | $La_2SiO_5$ |
| APS $La_2SiO_5$ Stand alone | 660°C/6 h to burn out graphite substrate | $La_2SiO_5 + La_2O_3$ |
| | annealed at 1100°C/4h | $La_2SiO_5 + La_2O_3$ |
| | 1150°C/20hc, 3 cycles | $La_2SiO_5 + La_2O_3$ (very minor) |

*annealing condition: 1150°C/4 h in Ar-5%$H_2$

** cyclic test condition: 1150°C/20h cycle (20 h high temperature, 20 min room temperature) in air

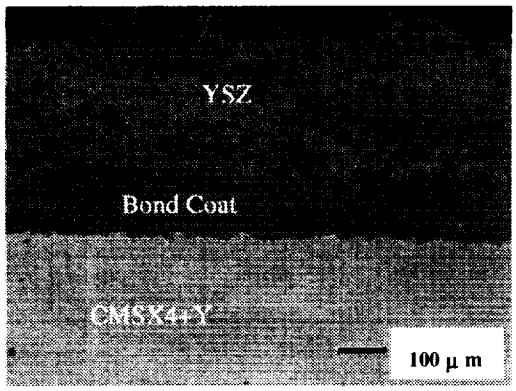


Fig. 1a As-sprayed standard YSZ

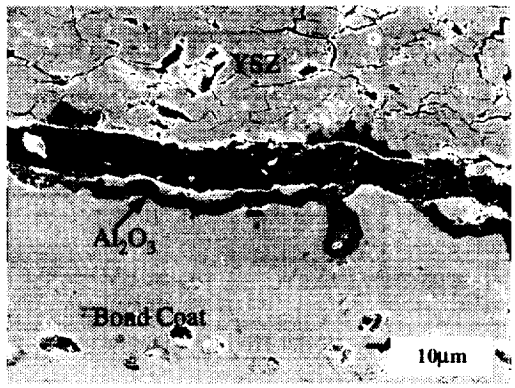


Fig. 1b Standard YSZ after 18- 20h cycles at 1150°C. Failure occurred mostly in YSZ near the YSZ/TGO boundary.

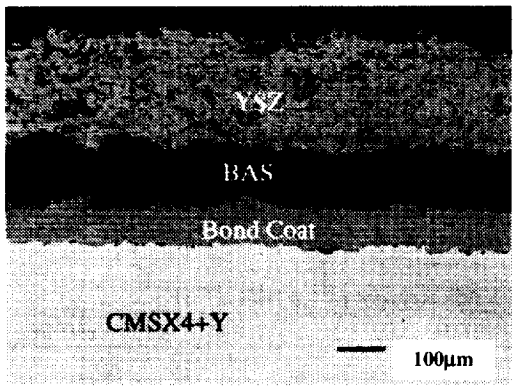


a. low magnification image

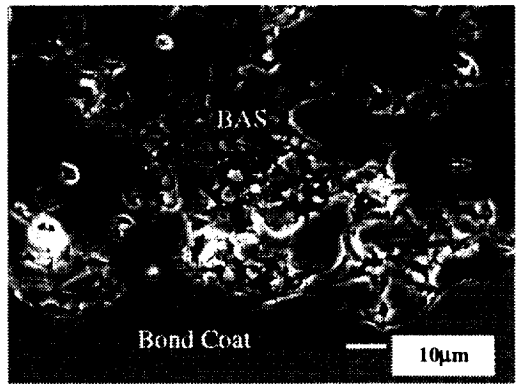


b. high magnification image

Fig. 2 As-sprayed HVOF BAS/YSZ. BAS coating is porous and incompletely melted.

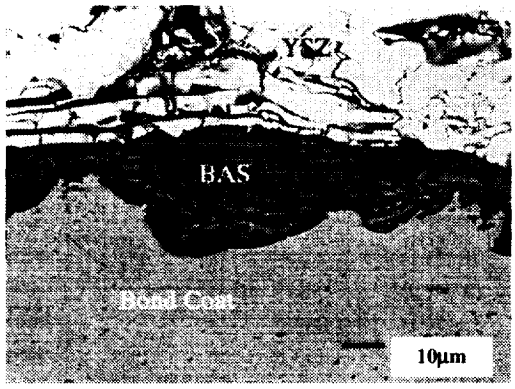


Fig. 3a As-sprayed APS BAS/YSZ. BAS coating has a layered structure.

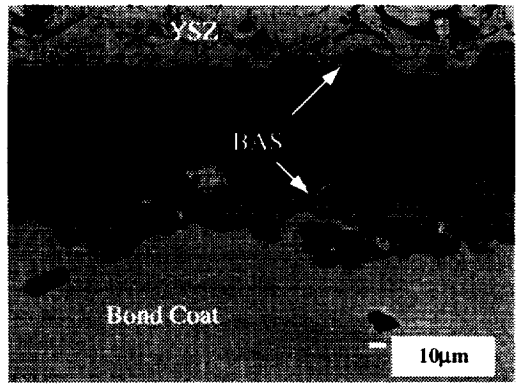


Fig. 3b APS BAS/YSZ failed after 2-20h cycles at 1150°C. Failure occurred along BAS/YSZ interface.

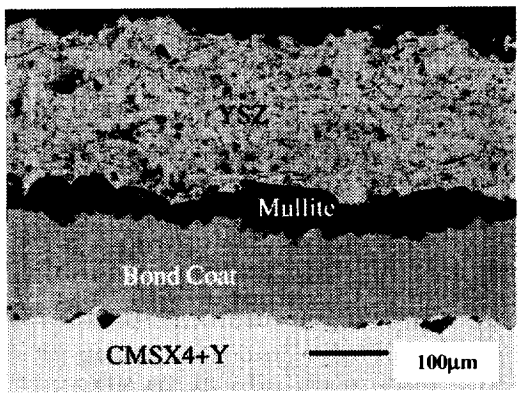


Fig. 4a As-sprayed APS mullite/YSZ

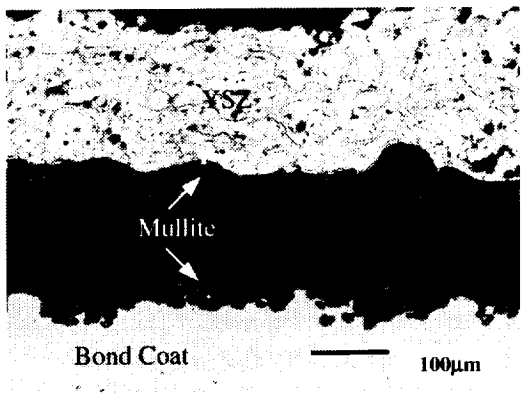


Fig. 4b APS mullite/YSZ failed after 1- 20h cycles at 1150°C. Mullite coating cracked and failure occurred inside mullite coating.

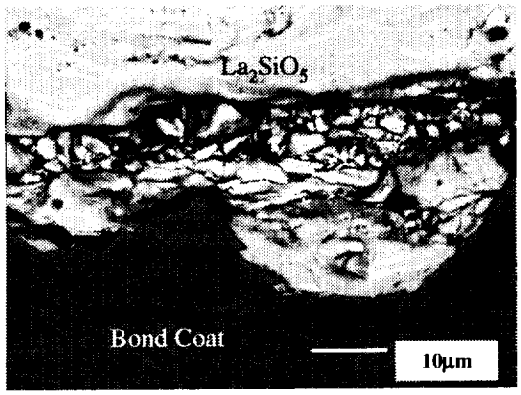


Fig. 5a As-sprayed HVOF $La_2SiO_5$/YSZ. $La_2SiO_5$ coating is porous and incompletely melted.

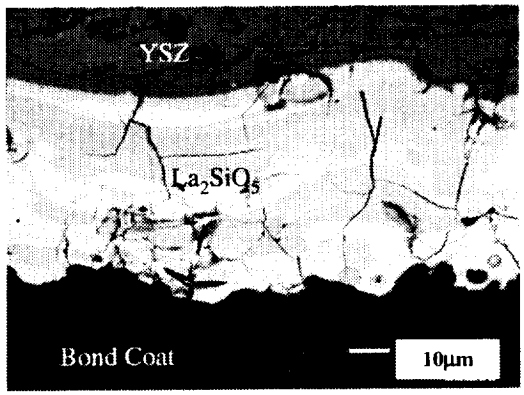


Fig. 5b As-sprayed APS $La_2SiO_5$/YSZ. $La_2SiO_5$ coating is denser but cracked.

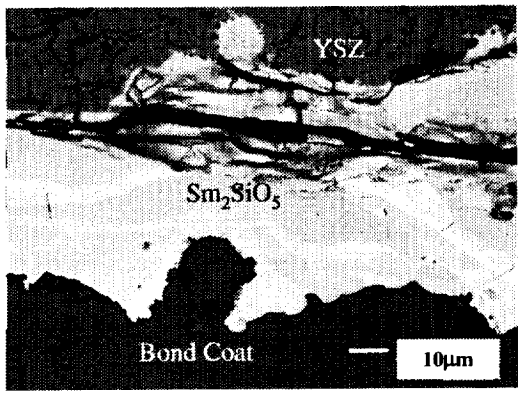


Fig. 6a As-sprayed APS $Sm_2SiO_5$/YSZ on heated substrate. Large cracks developed in the $Sm_2SiO_5$ coating.

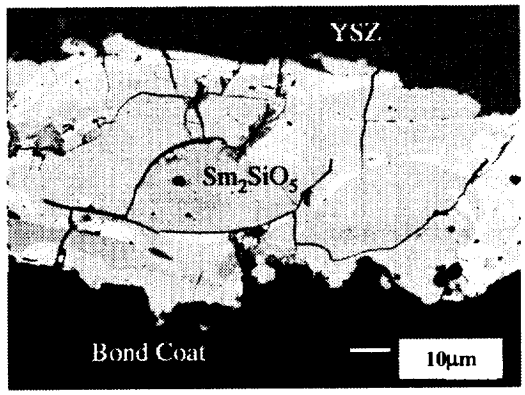


Fig. 6b As-sprayed APS $Sm_2SiO_5$/YSZ on unheated substrate. Microcracks developed in the $Sm_2SiO_5$ coating

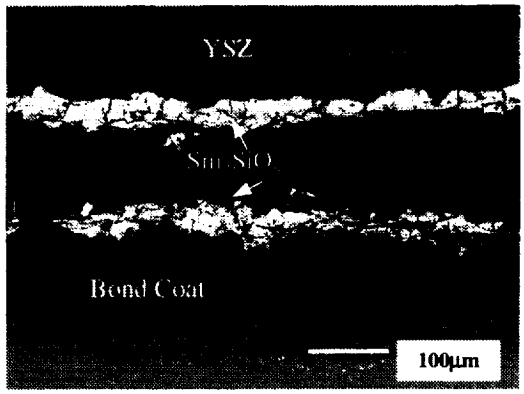


Fig. 6c APS $Sm_2SiO_5$/YSZ on unheated substrate after 3-20h cycles at 1150°C. Failure occurred in the $Sm_2SiO_5$ coating.

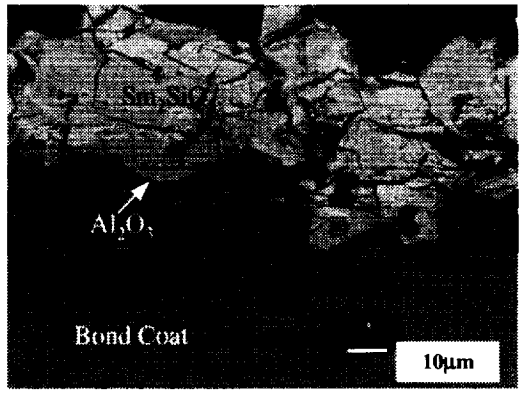


Fig. 6d High magnification image of 6c. More cracks developed in the $Sm_2SiO_5$.

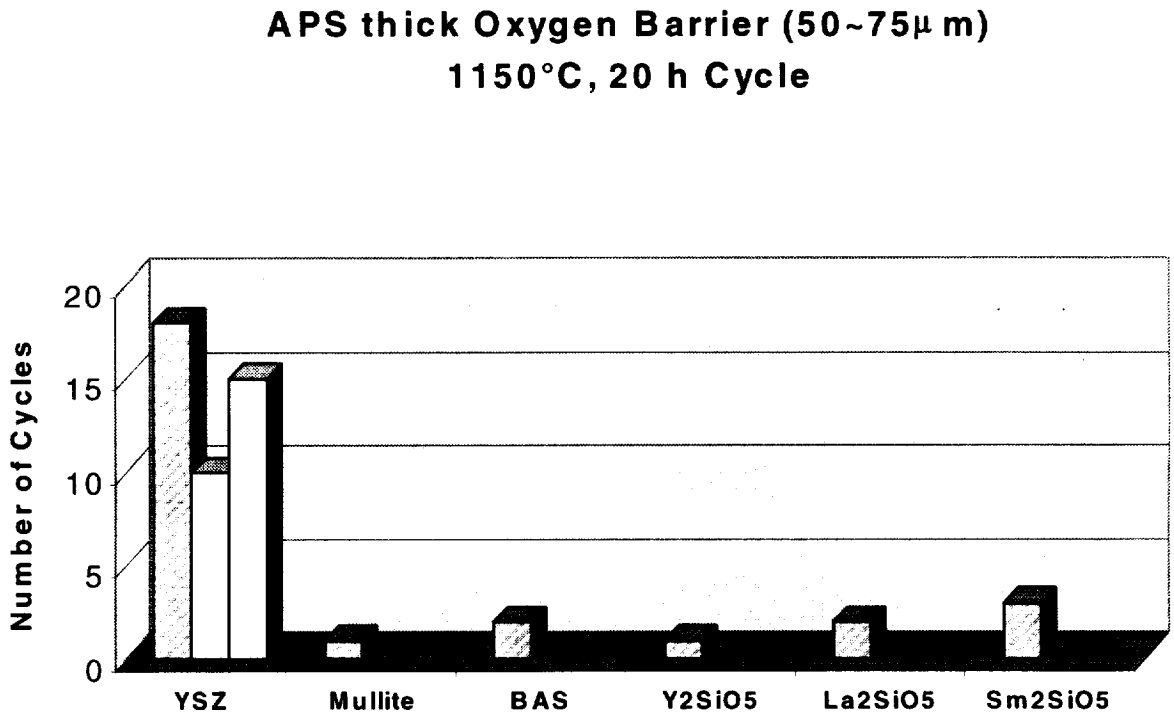


Fig. 7 Cyclic oxidation durability of thick APS oxygen barrier/YSZ TBCs. Each bar represents one tested specimen.

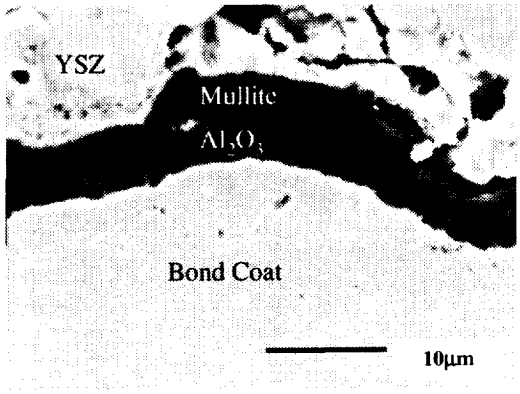


Fig. 8a Cross section of 3μm mullite/YSZ after 8-20h cycles at 1100°C. Dense $Al_2O_3$ formed underneath mullite coating.

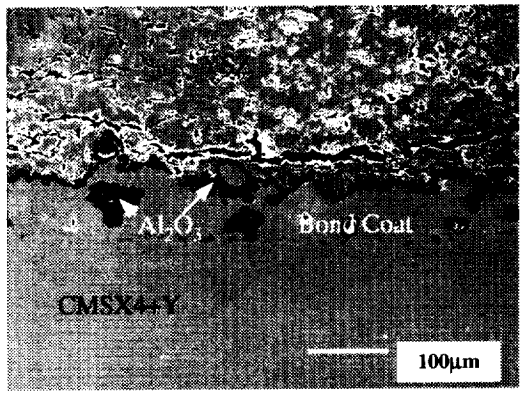


Fig. 8b low magnification image of 8a. Failure occurred in YSZ, similar to the failure mode of standard YSZ.

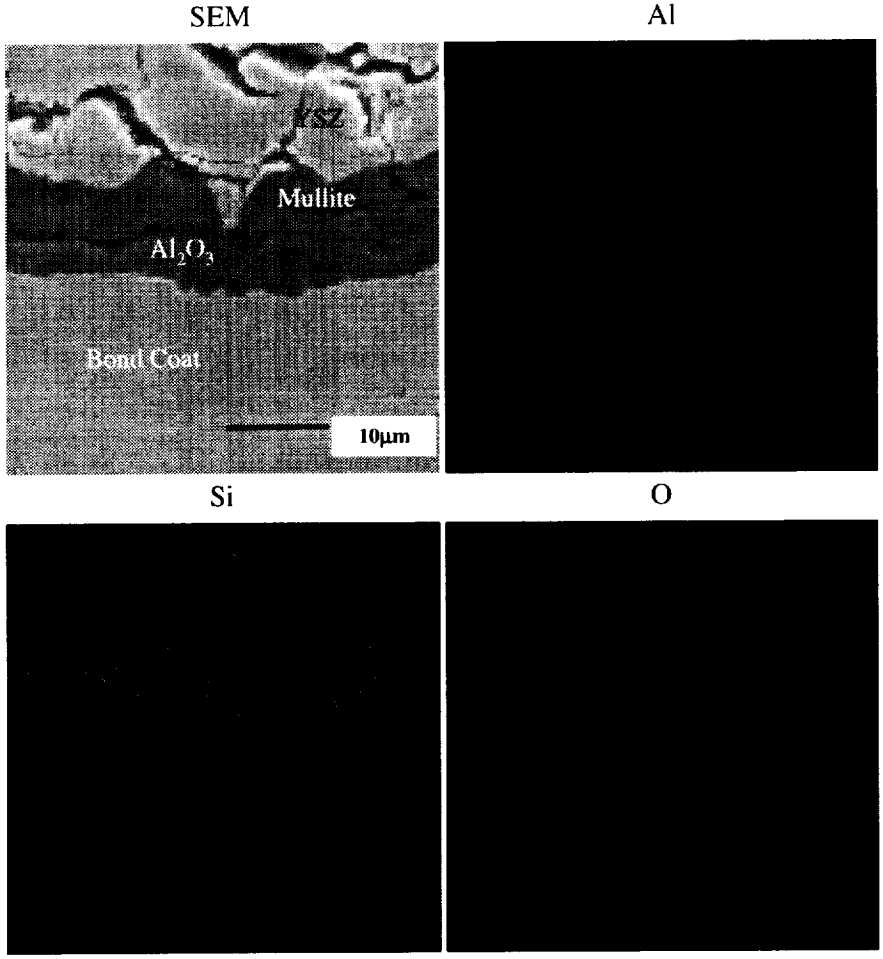


Fig. 9 Cross section and X-ray mapping for Al, Si and O of 6μm mullite/YSZ after 13-20h cycles at 1100°C.

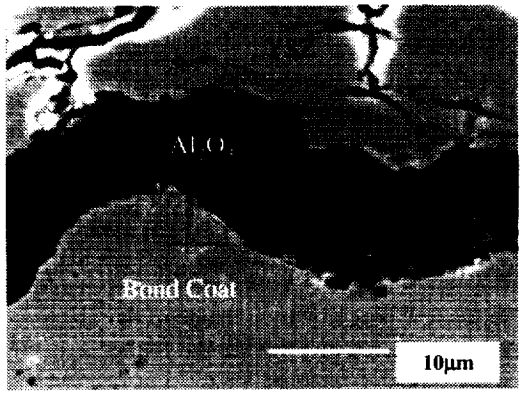


Fig. 10a Standard YSZ after 11-20h cycles at 1100°C.

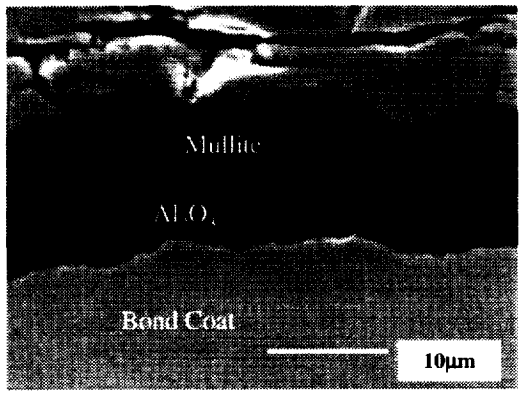


Fig. 10b 6μm mullite/YSZ after 13-20h cycles at 1100°C. The thickness of $Al_2O_3$ is about 1/2 of that formed in the standard YSZ.

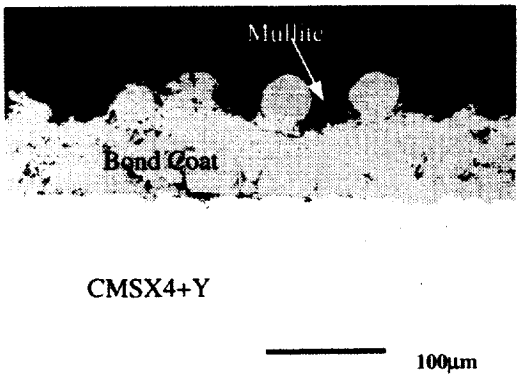


Fig.11a As sprayed SPPS mullite. Mullite completely covered the rough surface of the bond coat.

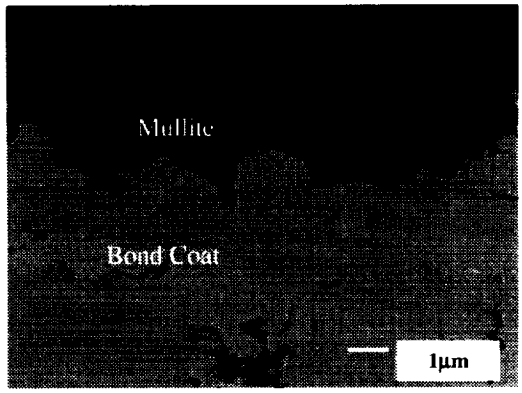


Fig. 11b High magnification image of 11a

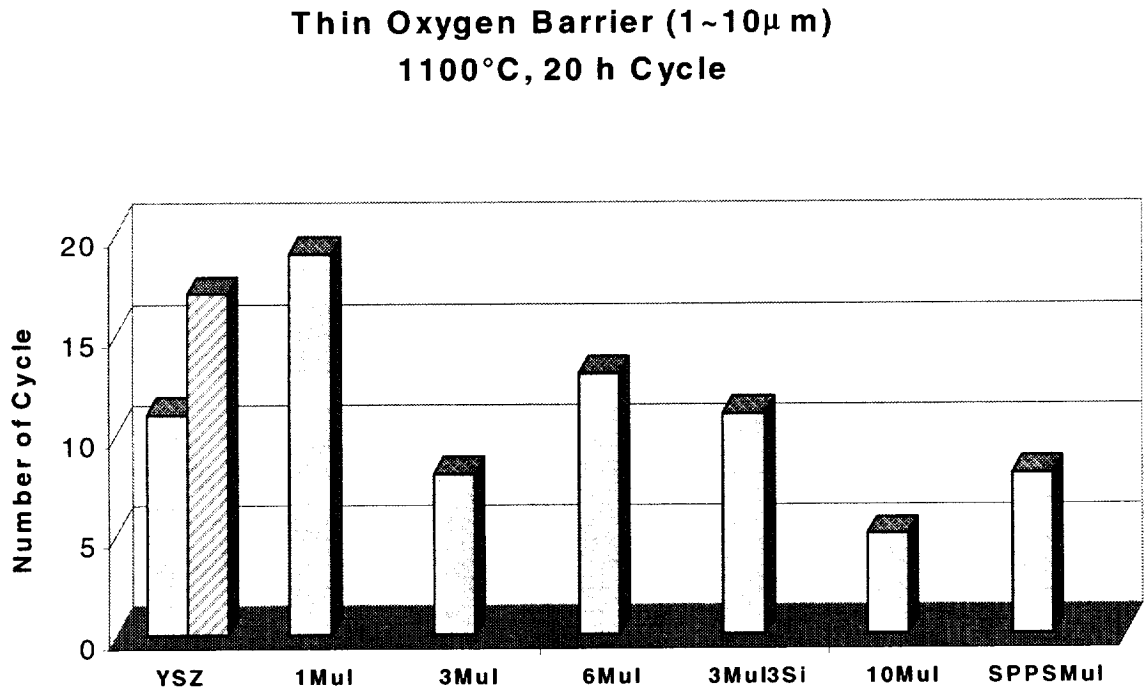


Fig. 12 20h cyclic oxidation durability of thin oxygen barrier/YSZ TBCs at 1100°C. Each bar represents one tested specimen.

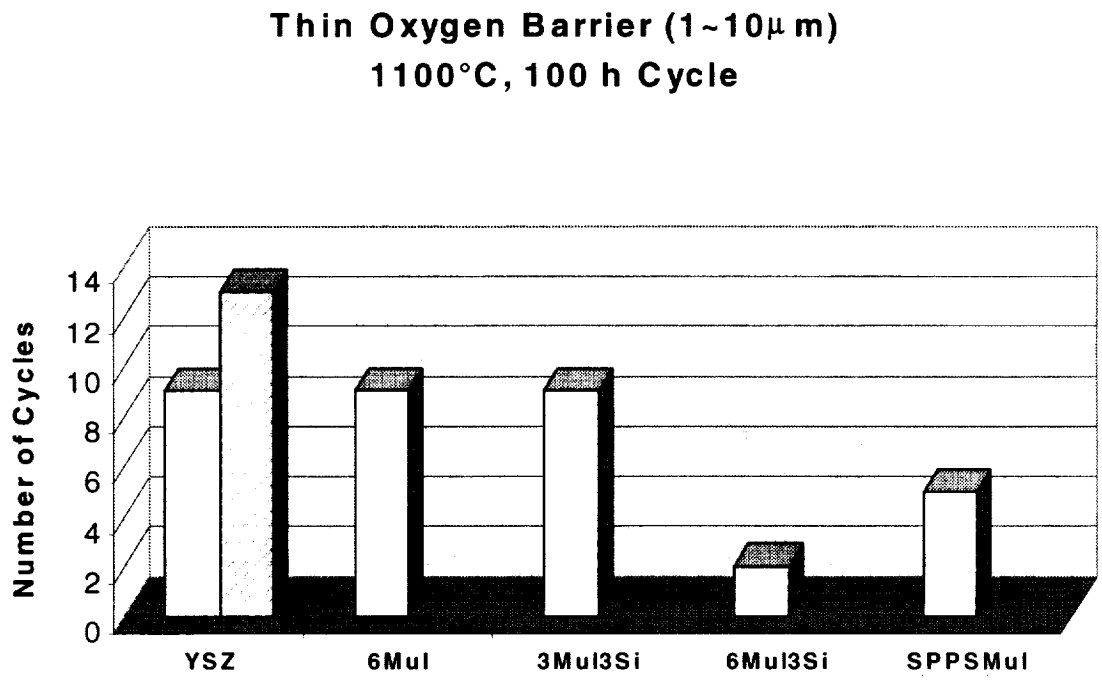


Fig. 13. 100h cyclic oxidation durability of thin oxygen barrier/YSZ TBCs at 1100°C. Each bar represents one tested specimen.

# REPORT DOCUMENTATION PAGE

*Form Approved*
*OMB No. 0704-0188*



| 1. AGENCY USE ONLY (*Leave blank*) | 2. REPORT DATE | 3. REPORT TYPE AND DATES COVERED |
|---|---|---|
| | July 1999 | Technical Memorandum |

**4. TITLE AND SUBTITLE**

Development of Refractory Silicate-YSZ Dual Layer TBCs

**5. FUNDING NUMBERS**

WU-537-04-23-00

**6. AUTHOR(S)**

Yirong He, Kang N. Lee, Surendra Tewari, and Robert A. Miller

**7. PERFORMING ORGANIZATION NAME(S) AND ADDRESS(ES)**

National Aeronautics and Space Administration
John H. Glenn Research Center at Lewis Field
Cleveland, Ohio 44135-3191

**8. PERFORMING ORGANIZATION REPORT NUMBER**

E-11661

**9. SPONSORING/MONITORING AGENCY NAME(S) AND ADDRESS(ES)**

National Aeronautics and Space Administration
Washington, DC 20546-0001

**10. SPONSORING/MONITORING AGENCY REPORT NUMBER**

NASA TM—1999-209079

**11. SUPPLEMENTARY NOTES**

Yirong He, Kang N. Lee, and Surendra Tewari, Cleveland State University, Cleveland, Ohio 44115 (work funded under NASA Cooperative Agreement NCC3-445); Robert A. Miller, NASA Glenn Research Center. This work was supported by DOE AGTSR program under the contract number 96-01-SR042 and other NASA contribution. Responsible person, Robert A. Miller, organization code 5160, (216) 433-3298.

**12a. DISTRIBUTION/AVAILABILITY STATEMENT**

Unclassified - Unlimited
Subject Category: 27 Distribution: Nonstandard

This publication is available from the NASA Center for AeroSpace Information, (301) 621-0390.

**12b. DISTRIBUTION CODE**

**13. ABSTRACT** ***(Maximum 200 words)***

Development of advanced thermal barrier coatings (TBCs) is the most promising approach for increasing the efficiency and performance of gas turbine engines by enhancing the temperature capability of hot section metallic components. Spallation of the yttria-stabilized zirconia (YSZ) top coat, induced by the oxidation of the bond coat coupled with the thermal expansion mismatch strain, is considered to be the ultimate failure mode for current state-of-the-art TBCs. Enhanced oxidation resistance of TBCs can be achieved by reducing the oxygen conductance of TBCs below that of thermally grown oxide (TGO) alumina scale. One approach is incorporating an oxygen barrier having an oxygen conductance lower than that of alumina scale. Mullite, rare earth silicates and glass ceramics have been selected as potential candidates for the oxygen barrier. This paper presents the results of cyclic oxidation studies of oxygen barrier/YSZ dual layer TBCs.

**14. SUBJECT TERMS**

TBC; Mullite; Silicates; Oxygen barrier; APS; Small particle plasma spray; Sputtering; Life

**15. NUMBER OF PAGES**

20

**16. PRICE CODE**

A03

| 17. SECURITY CLASSIFICATION OF REPORT | 18. SECURITY CLASSIFICATION OF THIS PAGE | 19. SECURITY CLASSIFICATION OF ABSTRACT | 20. LIMITATION OF ABSTRACT |
|---|---|---|---|
| Unclassified | Unclassified | Unclassified | |